Ultrasensitive nonlinear vibrational spectroscopy of complex molecular systems

Selig, O.

Publication date
2017
Document Version
Other version
License
Other

Chapter 4

Temperature-Induced Collapse of Elastin-Like Peptides Studied by 2DIR Spectroscopy

Elastin-like peptides (ELP) are hydrophobic biopolymers that exhibit a reversible coacervation transition when the temperature is raised above a critical point. Here we use a combination of linear infrared spectroscopy, two-dimensional infrared (2DIR) spectroscopy and molecular dynamics simulations to study the structural dynamics of two elastin-like peptides. Specifically, we investigate the effect of the solvent environment and temperature on the structural dynamics of a short (5-residue) elastin-like peptide and of a long (450-residue) elastin-like peptide. We identify two vibrational energy transfer processes that take place within the amide I′ band of both peptides. We observe that the rate constant of one of the exchange processes is strongly dependent on the solvent environment and argue that the coacervation transition is accompanied by a desolvation of the peptide backbone where up to 75% of the water molecules are displaced. We also study the spectral diffusion dynamics of a valine residue that is present in both peptides. We find that these dynamics are relatively slow and are indicative of an amide group that is shielded from the solvent. We conclude that the coacervation transition of elastin-like peptides is probably not associated with a conformational change involving this residue.

4.1 INTRODUCTION

Elastin is the protein which provides elasticity to many mammalian tissues, such as the lungs,[86–88] skin[89–91] and arteries.[89,92,93] Inside these tissues elastin is present as elastic fibers formed by the self-assembly of the precursor protein tropoelastin (mature elastin fibers result from the enzymatic cross-linking of tropoelastin molecules). The properties of (tropo)elastin are intimately linked to its special structure which consists of alternating hydrophilic and hydrophobic domains.[94] The hydrophilic domains are the regions where the cross-links occur while the hydrophobic domains turn out to play a crucial role in the self-assembly process. These hydrophobic regions consist of short stretches of amino-acid residues that are repeated many times and adopt a disordered conformation.[94] An example of such a repetitive sequence encountered in elastin is the pentapeptide repeat (Val-Pro-Gly-Val-Gly)$_n$. Interestingly, synthetic polypeptides based on this repeating sequence, also known as elastin-like peptides (ELP), can excellently mimic specific properties of elastin.[95–97] For instance, solutions of ELPs display an inverse temperature transition around 37 °C: at low temperatures ELPs are highly soluble in water while they reversibly aggregate when the temperature is increased beyond the transition temperature. This phenomenon, also referred to as coacervation, is thought to lie at the origin of the self-assembly of elastin. In addition to forming an excellent model system for studying the self-assembly of elastin, elastin-like peptides have attracted considerable research interest because of their application perspective in, for example, tissue engineering[98,99] and drug delivery.[100,101]

The molecular mechanism underlying the inverse temperature transition of elastin-like peptides is not well understood. Pioneering work by Urry et al.[95,102] suggested that the coacervation may be due to the formation of a β-turn between the two valine residues within the pentapeptide repeat unit (i.e. around the Pro-Gly fragment). These researchers hypothesized that the formation of a high density of β-turns would force the disordered peptide conformation (observed below the transition temperature) into a conformation displaying long-range order, termed a β-spiral.[103,104] However, the existence of the β-spiral remains highly speculative as molecular dynamics simulations indicate that this structure is not stable in water.[105,106] In the past a variety of spectroscopic techniques, including infrared,[107–109] Raman,[110,111] NMR[102,112,113] and circular dichroism[95,96,109,114] spectroscopy, have been used to study the coacervation transition in ELPs. However, obtaining a detailed molecular picture of the coacervation mechanism has proven extremely difficult. The main challenge lies in the fact that ELPs populate a large ensemble of disordered conformations which, moreover, interconvert on very short timescales (down to nanoseconds).[115] Ultrafast spectroscopic methods are in principle well suited to characterize the disordered conformational ensemble of ELPs because they probe molecular structures on timescales short with respect to the interconversion time. Recently Tokmakoff and coworkers used 2DIR spectroscopy in combination with computational methods to study the structure of a number of very short elastin-like peptides (i.e. consisting of a single repeat unit).[116,117] The authors found that the ELPs studied can indeed adopt a β-turn, but the β-turn turned out to be very labile, with the result that only a small fraction of the molecules adopts

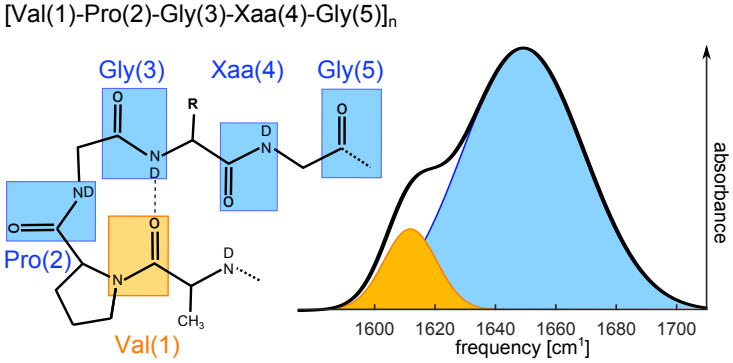

FIGURE 4.1. Chemical structure and typical infrared spectrum of elastin-like peptides in D_2O. The amide I′ groups are indicated with rectangles. The resonance at 1615 cm^{-1} (orange) originates from the amide I′ mode of the Val(1) residue, and the mode at 1650 cm^{-1} (blue) is attributed to the amide I′ mode of the other four residues.

the β-turn. It should be noted that because of their short length the ELPs in question did not exhibit a coacervation transition. As a result the exact role of the β-turn in the coacervation transition of ELPs is not resolved.

In this work we use 2DIR spectroscopy to study the coacervation transition of ELPs. This chapter is divided into two parts. The first part deals with a 450-residue ELP of the type $(Val(1)\text{-}Pro(2)\text{-}Gly(3)\text{-}Xaa(4)\text{-}Gly(5))_n$. Here Xaa represents a guest residue that can be any residue except proline. This ELP displays a sharp coacervation transition, and the transition temperature can be tuned by varying the hydrophobicity of the Xaa residue. We will specifically focus on spectroscopic observables that report on the local fluctuations experienced by the peptide, such as vibrational energy transfer rates and spectral diffusion rates. These observables provide information about the interaction of the peptide with its solvation shell, and we will study how this interaction changes as a function of temperature. In the second part of the chapter we will draw a parallel between the behavior of this long ELP and that of a very short ELP, which is composed of the single pentapeptide repeat Val-Pro-Gly-Val-Gly. This latter ELP does not display a coacervation transition. Nevertheless, it serves as a good model system for studying the conformational flexibility of longer ELPs. In this case we will modify the solvation shell of the peptide, and thereby likely also its secondary structure, by adding the amphiphilic trifluoroethanol (TFE) as a cosolvent. TFE is known to enhance secondary structural elements in peptides.[118,119] By comparing the effects of temperature and solvent composition on the ELPs studied, we gain insight into the mechanism of the coacervation transition.

4.2 MATERIALS AND METHODS

4.2.1 SAMPLE

Fig. 4.1 provides a general overview of the chemical structure of elastin-like peptides and illustrates the basic features observed in the infrared spectrum of this class of peptides. The two different elastin-like peptides investigated in this work are referred to as ELP90 and ELP1. ELP90 is a 90-repeat elastin-like peptide described by the sequence $(\text{Val-Pro-Gly-Xaa-Gly})_{90}$ where the guest position Xaa is occupied by the residues Val, Leu and Gly in a 5:2:3 ratio. ELP90 was synthesized using recombinant-DNA techniques as previously documented.[120] The peptide was purified using inverse transition cycling[121] and its purity was checked by SDS-PAGE. For the spectroscopic measurements the peptide was dissolved in D_2O (Cambridge Isotopes Laboratories, Inc.) at concentrations ranging from 10 mg/ml to 60 mg/ml.
ELP1 stands for the single-repeat pentapeptide Ac-Val-Pro-Gly-Val-Gly-NH_2. The peptide was custom-synthesized by GL Biochem (Shanghai, China). In order to remove residual trifluoroacetic acid (TFA) the peptide was dissolved in DCl and lyophilized before use.[122] The spectroscopic measurements were perfomed on solutions of ELP1 (25 mg/ml) in TFE:D_2O mixtures (trifluoroethanol-d3, Sigma-Aldrich). In these experiments the volume fraction of TFE was varied from 0% to 65%.

4.2.2 INFRARED SPECTROSCOPY

Linear infrared spectroscopy All linear absorption measurements were performed using a Bruker Vertex 80v FTIR spectrometer equipped with a liquid-nitrogen-cooled mercury-cadmium-telluride (MCT) detector. The spectra were recorded under a N_2 atmosphere at a resolution of 2 cm^{-1}. For every spectrum 50 scans were averaged. In all measurements a standard sample cell with a path length of 50 μm was used. The reported spectra were corrected for the absorption of the (TFE:D_2O) solvent background. The temperature-dependent FTIR measurements on ELP90 were performed using a peltier-cooled temperature cell (Mid-IR Falcon, Pike technologies). The temperature was ramped from 293 K to 323 K at a rate of 0.4 K/min, and the spectra were acquired at intervals of 2 K. The background measurements on neat D_2O were performed using the same ramping parameters.

Two-dimensional infrared spectroscopy The experimental setup used in the experiments is described in Chapter 3. The pump and probe pulses are centered at $\sim$1650 cm^{-1}, in resonance with the amide I′ vibration. All experiments are performed under an N_2 atmosphere and with the help of a standard sample cell with a path length of 50 μm. The temperature of the ELP90 samples is kept at 296 K and 318 K using a peltier element with an active feedback loop.

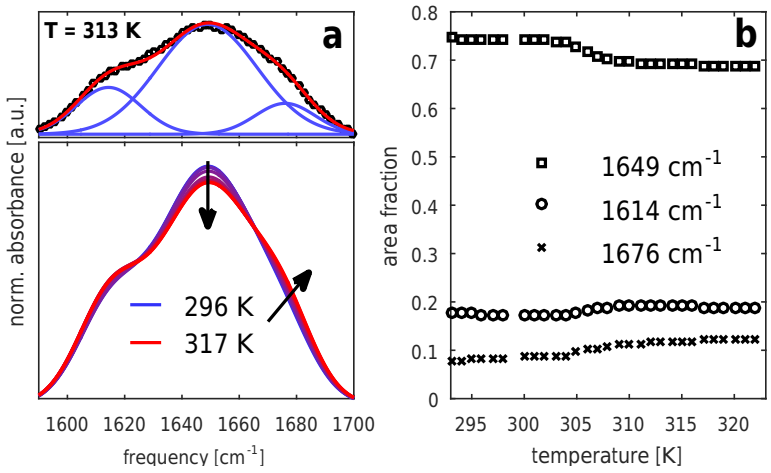

FIGURE 4.2. a) Linear infrared spectra of ELP90 in D_2O (20 mg/ml) for temperatures between 296 K and 317 K. The top panel illustrates the decomposition of the spectrum at 313 K (black squares) into three Gaussian bands (blue lines). The red solid line represents the sum of the three Gaussians. b) Relative contributions of the three bands to the amide I′ spectrum of ELP90 as a function of temperature. The relative contribution is expressed as the integrated intensity of the respective band divided by the integrated intensity of the amide I′ spectrum.

4.3 RESULTS

4.3.1 EFFECT OF TEMPERATURE ON THE STRUCTURAL DYNAMICS OF ELP90

LINEAR INFRARED SPECTRA We start by characterizing the temperature-induced collapse of ELP90 using conventional FTIR spectroscopy. Figure 4.2 displays linear infrared spectra of ELP90 recorded at a range of temperatures starting at ∼15 K below until ∼15 K above the transition temperature. The ELP90 spectrum clearly exhibits two resonances as is schematically illustrated in Fig. 4.1: the redshifted resonance at 1615 cm^{-1} is attributed to the amide group of Val(1), and the resonance at 1650 cm^{-1} is due to the other four amide groups in the pentapeptide repeat. Upon increasing the temperature the peak absorbance at 1650 cm^{-1} decreases, and an increased absorption develops around 1675 cm^{-1} . In order to quantify these spectral changes we use a fitting procedure to deconvolute the ELP90 spectra into Gaussian bands (Figure 4.2a). It turns out that three Gaussians are required to adequately describe the IR spectra at all temperatures. The Gaussian bands are centered at 1614 cm^{-1}, 1649 cm^{-1}, and 1676 cm^{-1} and have full-width-at-half-maxima (FWHM) of 24 cm^{-1}, 41 cm^{-1}, and 24 cm^{-1}, respectively. In the fitting procedure only the amplitudes of the bands are allowed to vary as a function of temperature (their center position and FWHM remain fixed). Figure 4.2 shows the integrated intensity of these bands as a function of temperature. All bands show a sigmoidal dependence on temperature with a transition point at 305 K. The sigmoidal temperature dependence

clearly indicates that the temperature-induced aggregation is a two-state transition.

TWO-DIMENSIONAL INFRARED SPECTRA In order to gain more insight into the origin of the different bands observed in the linear infrared spectrum of ELP90, we performed 2DIR experiments on the peptide. Figure 4.3 displays the (delay-dependent) 2DIR spectra of ELP90 recorded at temperatures below (296 K; left-hand side) and above (318 K; right-hand side) the transition temperature. We first consider the low-temperature 2DIR spectra. At short delays (0.3 ps) we observe a diagonally elongated lineshape, which indicates that the amide I′ spectrum is strongly inhomogeneously broadened. The 2DIR spectrum consists of a negative component on the diagonal, due to ground-state bleaching and stimulated emission of the $0\rightarrow1$ transition, and a positive component at lower probe frequencies, due to the induced absorption of the $1\rightarrow2$ transition. Contrary to the FTIR spectrum, in the 2DIR spectrum the Val(1) band shows up as a well separated resonance at 1615 cm^{-1}. The other subbands constituting the amide I′ spectrum overlap and give rise to one broad resonance around 1660 cm^{-1}. As the pump-probe delay is increased, two effects are observed. Firstly, we see that cross-peaks appear between the Val(1) band and the band at 1660 cm^{-1}. These ingrowing cross-peaks point at vibrational energy transfer between the Val(1) mode and the mode at 1660 cm^{-1}. The appearance of cross-peaks on both sides of the diagonal demonstrates that both uphill and downhill energy transfer processes occur. The second effect observed with increasing pump-probe delay is the spectral reshaping of the band around 1660 cm^{-1}: from a diagonally elongated lineshape at short delays to a round lineshape at long delays.

Next we consider the changes that occur upon increasing the temperature above the transition point. For short delays (0.3 ps) we observe the appearance of a pronounced blue shoulder at $\sim$1675 cm^{-1}. The delay-dependence of the 2DIR spectra is the same as observed at temperatures below the transition point. Cross-peaks develop between the high-frequency band and the Val(1) band; and the shape of the 1660 cm^{-1} band evolves from diagonal to round. In Figure 4.4a we compare the delay dependence of the 2DIR signals at three positions along the diagonal that correspond to the center positions of the three main bands identified in the linear spectra. Figure 4.4a shows that the relaxation of the amide I′ mode speeds up with decreasing frequency of the vibration, and that the relaxation rate does not depend on the aggregation state of the peptide.

RELAXATION AND EXCHANGE DYNAMICS In the previous section we have identified two energy transfer processes. In the first process energy is transferred to and from the Val(1) residue, and in the second process energy is exchanged between the two high frequency modes (reshaping of the $\sim$ 1650 cm^{-1} band). We can assign time constants to these two exchange processes by fitting a relaxation model to our data. The relaxation model used is summarized in Figure 4.5. The model describes the time-dependent populations of the three bands identified in the linear spectrum. These modes exchange population with each other and lose population through vibrational relaxation. The vibrational relaxation of the three modes proceeds via an intermediate state to a so-called hot ground state. The hot ground state accounts for the fact that vibrational relaxation leads to a slight increase in the sample temperature (which in turn affects the amide I′ spectrum).[123] The intermediate state serves to

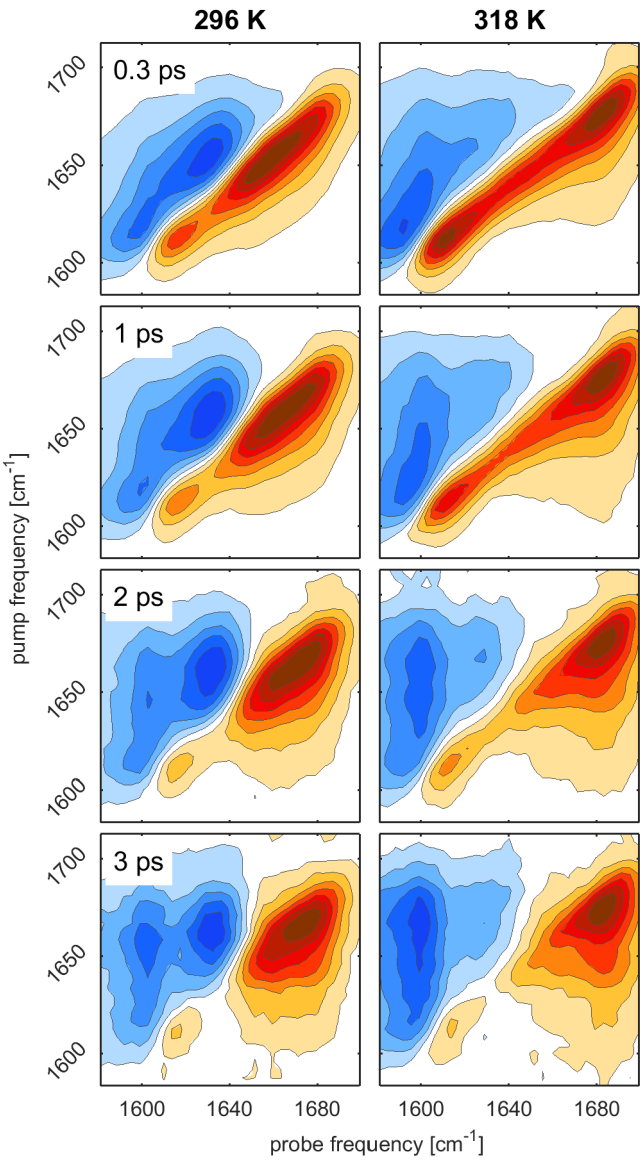

FIGURE 4.3. Isotropic 2DIR spectra of ELP90 in D_2O (20 mg/ml) at different pump-probe delays and for two different temperatures. Negative absorption changes are depicted in red, positive absorption changes in blue. The contour lines are drawn equally spaced at 12,5% increments.

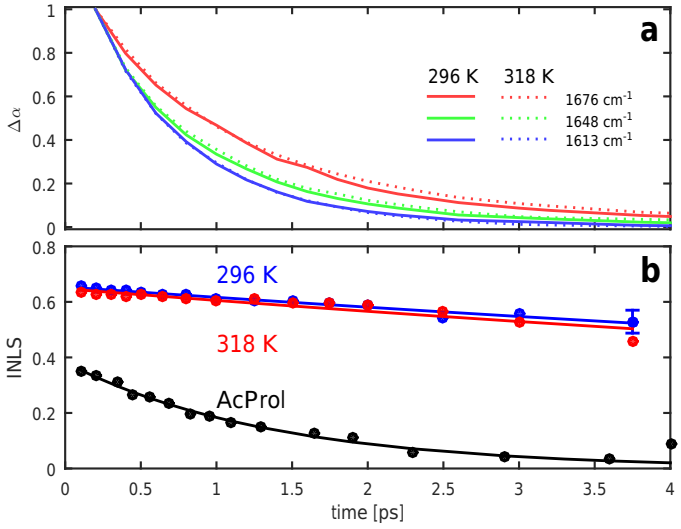

FIGURE 4.4. a) Time-dependent signal corresponding to three different frequencies on the diagonal of the 2DIR spectra of ELP90 for two different temperatures. b) Inverse nodal line slope (INLS) of the Val(1) resonance of ELP90 above (red) and below (blue) the transition temperature. For comparison, the INLS of acetylated proline in D_2O is shown in black.

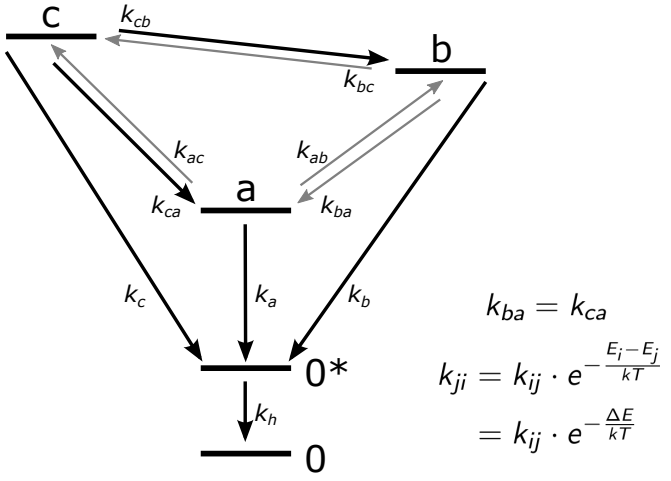

FIGURE 4.5. Schematic representation of the model used to describe the exchange dynamics of the amide I′ vibrations of ELP90 in D_2O. The three main modes identified in the linear infrared experiments are used to represent the amide I′ band: $a = 1613$ cm^{-1}, $b = 1648$ cm^{-1} and $c = 1675$ cm^{-1}. Thick arrows denote independent time constants and thin arrows denote time constants that are derived from the independent constants using the equations on the right.

describe the observation that sample heating is often slightly delayed with respect to the vibrational relaxation.[63] The time-dependent populations of the levels n_i (Figure 4.5) are governed by the following set of rate equations.

$$\frac{d}{dt}\begin{pmatrix} n_a \\ n_b \\ n_c \\ n_* \\ n_0 \end{pmatrix} = \begin{pmatrix} -k_a - k_{ab} - k_{ac} & k_{ba} & k_{ca} & 0 & 0 \\ k_{ab} & -k_b - k_{ba} - k_{bc} & k_{cb} & 0 & 0 \\ k_{ac} & k_{bc} & -k_c - k_{ca} - k_{cb} & 0 & 0 \\ k_a & k_b & k_c & -k_h & 0 \\ 0 & 0 & 0 & k_h & 0 \end{pmatrix} \cdot \begin{pmatrix} n_a \\ n_b \\ n_c \\ n_* \\ n_0 \end{pmatrix} \tag{4.1}$$

We assume that the uphill exchange rates are related to the downhill rates via the detailed-balance condition $k_{ji} = k_{ij}\exp\left(-\frac{E_i - E_j}{kT}\right) = k_{ij}\exp\left(-\frac{\Delta E}{kT}\right)$ where k is Boltzmann's constant, T is the absolute temperature and ΔE is the energy difference between the two modes. In order to further reduce the number of fitting parameters we assume that the exchange process with the Val(1) band is governed by a single time constant (that is we set $k_{ba} = k_{ca}$). We aim to describe the experimental 2DIR signal at three specific pump frequencies, specifically at the center frequencies of the three modes identified in the linear spectra. The 2DIR signal at these pump frequencies is given by

$$\Delta\alpha\left(\nu_{\mathrm{pu}}^{(\mathrm{i})}, \nu_{\mathrm{pr}}, t\right) = \sigma_{\mathrm{heat}}^{(\mathrm{i})}\left(\nu_{\mathrm{pr}}\right) \cdot n_0^{(\mathrm{i})}(t) + \sum_j R_{ij} \cdot \sigma_{\mathrm{j}}\left(\nu_{\mathrm{pr}}\right) \cdot n_j^{(\mathrm{i})}(t) \tag{4.2}$$

In this expression the indices i and j serve as mode labels, which run over the set $\{a, b, c\}$. ν_{pr} represents the probe frequency, and $\nu_{\mathrm{pu}}^{(i)}$ represents the center frequency of mode i. The transient spectrum associated with mode j is denoted as $\sigma_{\mathrm{j}}(\nu_{\mathrm{pr}})$ and can be obtained from the 2DIR spectrum at zero pump-probe delay (it is given by $\Delta\alpha(\nu_{\mathrm{pu}}^{(\mathrm{j})}, \nu_{\mathrm{pr}}, 0)$). The heating spectrum $\sigma_{\mathrm{heat}}^{(i)}(\nu_{\mathrm{pr}})$ is obtained from the 2DIR spectrum at long delays (the dependence on mode index i amounts to a scaling factor due to the variation of the sample absorbance with the pump frequency). We note that every pump frequency in the 2DIR spectrum is associated with a different set of time-dependent populations. This is because the initial conditions for the populations in Eqn. 4.1 depend on the pump frequency according to

$$n_j^{(\mathrm{i})}(0) = \delta_{ij}, \qquad n_0^{(i)}(0) = 0 \tag{4.3}$$

where δ_{ij} is the Kronecker delta. Finally we mention that the scaling factors R_{ij} are necessary to account for the different cross sections of the three modes. These 9 factors are not independent, and they can all be expressed in terms of the cross-section ratios of modes a to b and modes a to c (so that there are only two free parameters).

In summary, this model describes the time-dependence of the 2DIR spectrum (at three specific pump frequencies) in terms of 4 time-independent spectra that are directly extracted from the 2DIR spectrum (three mode spectra and one heating spectrum), and eight fitting parameters (three relaxation rates k_j, the heating rate k_{h}, two independent exchange constants k_{cb} and k_{ba}, and two independent scaling factors R_{ij}). Here we remark that, in fact, the two exchange constants, correspond directly

Temp. [K]	k_c [ps^{-1}]	k_b [ps^{-1}]	k_a [ps^{-1}]	k_{ba} [ps^{-1}]	k_{cb} [ps^{-1}]	k_{SD} [ps^{-1}]
296	0.55 ± 0.01	0.71 ± 0.02	1.04 ± 0.03	0.18 ± 0.02	0.38 ± 0.01	0.09 ± 0.02
318	0.54 ± 0.03	0.71 ± 0.05	1.04 ± 0.03	0.18 ± 0.02	0.31 ± 0.03	0.06 ± 0.02

TABLE I. Results of the fitting of the relaxation model to the ELP90 2DIR data. The rate constants reported are the result of averaging 5 independent measurement series per temperature. The errors give the standard deviation of the mean.

to the two exchange processes that were mentioned in our qualitative description of the 2DIR spectra: reshaping of the 1660 cm^{-1} band (k_{cb}) and energy transfer to and from the Val(1) band (k_{ba}).

We have fitted the relaxation model described above to a large number of ELP90 data sets, which were recorded both above and below the transition temperature. Figure 4.6 displays the fitting results for a typical data set. Note that in this figure the transient spectra have been normalized to emphasize the ingrowth of the cross peaks. We observe very good agreement between the experimental and the calculated spectra. Table I summarizes the rate constants extracted from the fits at both temperatures. We see that the relaxation constants and the exchange rate k_{ba} do not show a significant variation with the aggregation state of the peptide. Only the exchange between the two high-frequency modes (k_{cb}) shows a small but significant slowdown upon aggregation.

SPECTRAL DIFFUSION OF THE VAL(1) RESONANCE The 2DIR spectra in Figure 4.3 show that the Val(1) resonance (1615 cm^{-1}) is essentially decoupled from the rest of amide I′ band of ELP90. This resonance therefore reports on the local fluctuations experienced by the Val(1) residue. At short delays (0.3 ps) we see that the Val(1) resonance shows a pronounced diagonal elongation, which points to a strong inhomogeneous broadening of the resonance. It is interesting to consider how fast this inhomogeneity decays over time because the decay constant reflects the degree of solvent exposure of the respective residue: a fast decay corresponds to a solvent-exposed residue while a slow decay points to a residue that is shielded from the solvent.[27,76,124] We quantify the (time-dependent) inhomogeneity of the Val(1) resonance through the (inverse of the) slope of the nodal line. The time-dependence of this parameter is shown in Fig. 4.4b for temperatures above and below the transition temperature. We observe a very slow decay of the inverse nodal line slope at temperatures below the transition temperature, and, interestingly, this decay does not change upon aggregation of the peptide. As a reference experiment we have repeated these spectral diffusion measurements for a molecule which has an amide group that is fully solvent exposed. For this purpose we have chosen N-acetylated proline (AcPro) because its amide group has the same chemical environment as the amide group of the Val(1) residue in ELP90. As expected we see that for AcPro the inverse nodal line slope decays much faster compared to ELP90 (Figure 4.4b). These spectral diffusion measurements indicate that the amide group of the Val(1) residue

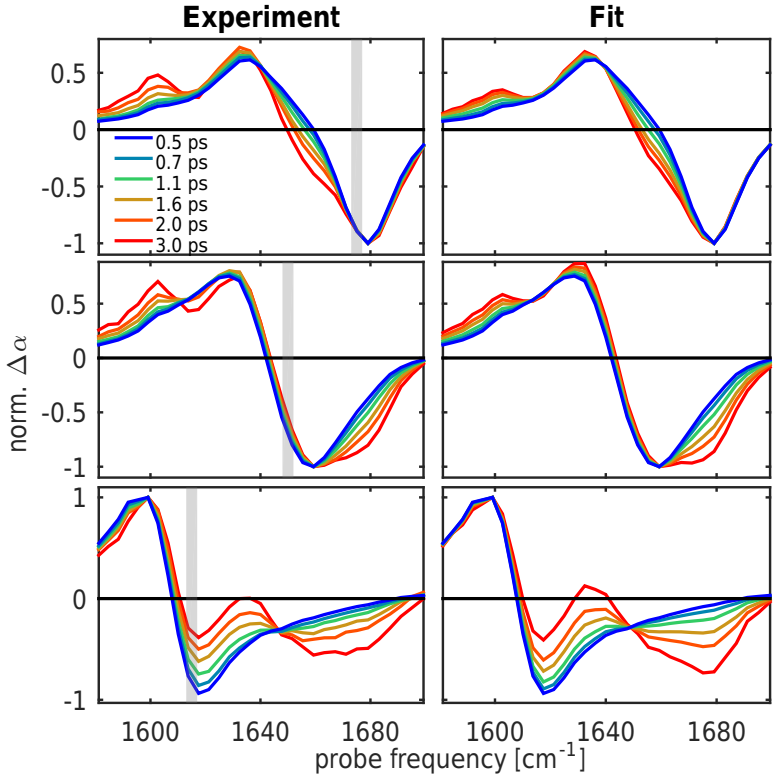

FIGURE 4.6. Comparison between the experimental (left) and calculated (right) pump slices for ELP90 (20 mg/ml) in D_2O below T_c (296 K). The pump frequencies are indicated by gray vertical bars and correspond to $\nu_{pump} = 1675$ cm^{-1}, 1648 cm^{-1} and 1615 cm^{-1}. The transient spectra are normalized to the maximum bleach (top and middle plots) or the maximum ESA (bottom plots) to emphasize the cross-peak dynamics.

is shielded from the solvent in both aggregation states of the peptide.

4.3.2 EFFECT OF THE SOLVENT COMPOSITION ON THE STRUCTURAL DYNAMICS OF ELP1

LINEAR INFRARED SPECTRA To gain more insight into the origin of the inverse temperature transition of ELP90 we performed additional experiments on the simpler ELP1 peptide, which is composed of a single pentapeptide repeat unit. Because ELP1 does not display a coacervation transition as a function of temperature, we decided to focus on possible conformational changes induced by the addition of the amphiphilic cosolvent trifluoroethanol (TFE). TFE is generally known to induce secondary structure in peptides.[125–127] In our experiments the solvent composition was varied from 0 to 65 volume percent TFE in D_2O [v/v%]. The FTIR spectra of these solutions are displayed in Figure 4.7. We have used the same global fitting

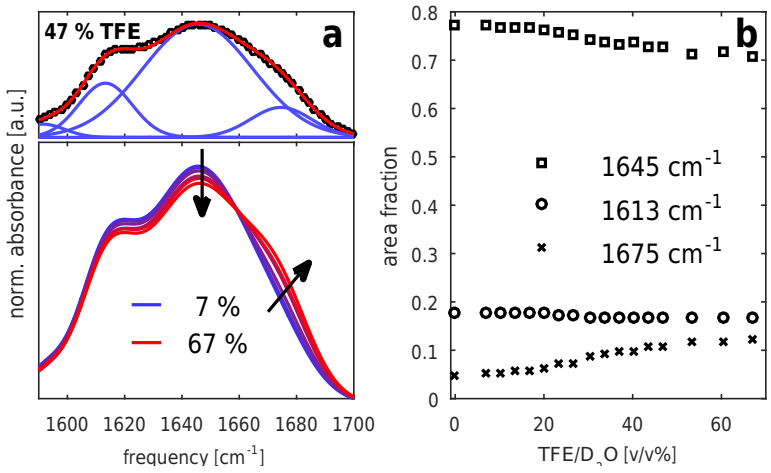

FIGURE 4.7. a) Linear infrared spectra of ELP1 (25 mg/ml) in TFE:D_2O mixtures of varying composition. The top panel illustrates the decomposition of a typical spectrum (black squares) into four Gaussian bands (blue lines). The red solid line represents the sum of the four Gaussians. b) Relative contribution of the three main bands to the amide I′ spectrum of ELP1 as a function of the solvent composition.

procedure as for ELP90 to decompose these spectra into Gaussian bands (Figure 4.7, top panel). The ELP1 amide I′ band can be excellently described using a linear combination of four Gaussians (centered around 1590 cm^{-1}, 1613 cm^{-1}, 1645 cm^{-1} and 1675 cm^{-1}). Three of the four bands have close to identical center positions as for ELP90. The fourth band at 1590 cm^{-1} is assigned to a carboxylic acid group due to incomplete amidation of the C-terminus of the pentapeptide. The intensity of this band is very small and it does not vary with solvent composition, so that we disregard the band in our analysis. Interestingly, the spectral evolution of ELP1 as a function of TFE concentration looks very similar to the spectral changes that were previously observed for ELP90 with increasing temperature.

2DIR SPECTROSCOPY Figure 4.8 shows the 2DIR spectra of ELP1 for two representative solvent compositions. We observe a number of effects in these spectra which parallel the observations made for ELP90. Firstly, the pronounced separation between the Val(1) band at 1615 cm^{-1} and the 1660 cm^{-1} band is clearly visible. Secondly, as a function of delay time we observe energy transfer between these two bands, as well as a reshaping of the 1660 cm^{-1} band. Finally, when considering the time dependence of the 2DIR signal (Fig. 4.9a) on the diagonal we observe a trend which is analogous to that of ELP90. Specifically, the relaxation speeds up with increasing redshift of the amide I′ vibration, but it is independent of the solvent composition.

RELAXATION AND EXCHANGE DYNAMICS We use the same relaxation model that we used above in our analysis of the ELP90 data, to quantitatively describe

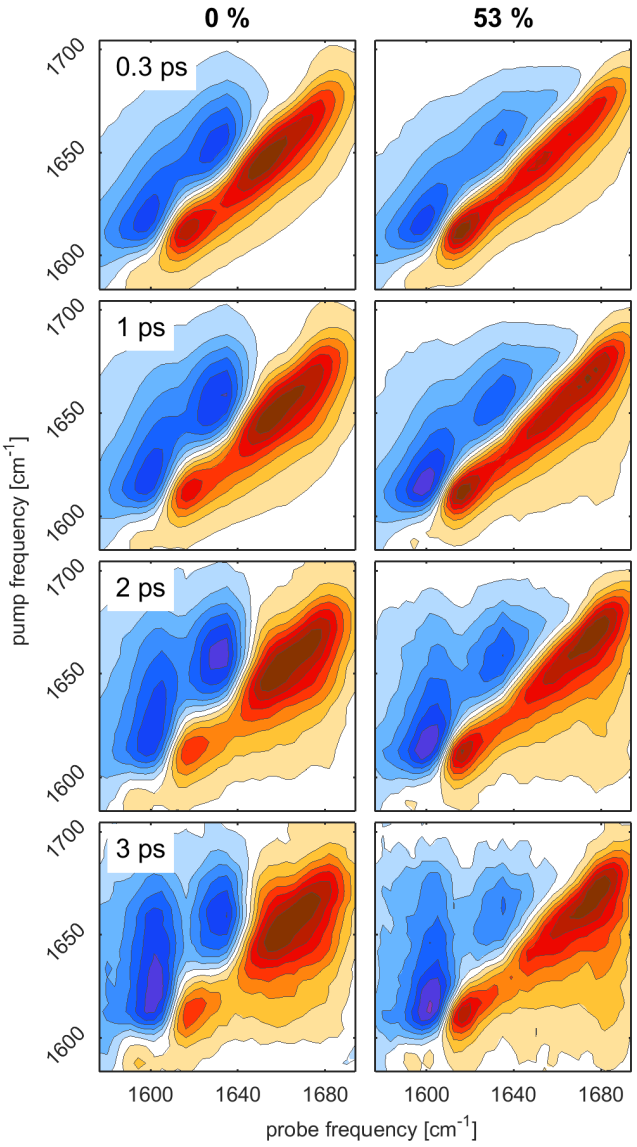

FIGURE 4.8. Isotropic 2DIR spectra of ELP1 (25 mg/ml) in TFE:D_2O mixtures at different pump-probe delays and for two solvent compositions: 0% TFE (left) and 53% TFE (right). Negative absorption changes are depicted in red, positive absorption changes in blue. The contours are drawn equally spaced at 12.5 % increments.

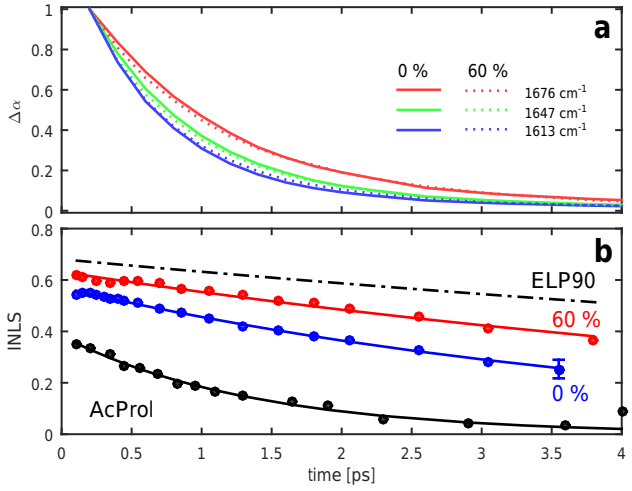

FIGURE 4.9. a) Time dependent bleaching signal extracted from the 2DIR spectra of ELP1 (25 mg/ml) in TFE:D_2O mixtures. The decay traces are shown for solvent mixtures at a low (0%, straight lines) and at a high (60%, dotted lines) volume fraction of TFE. The three colors correspond to the three modes, as indicated in the legend. b) Inverse nodal line slope (INLS) of Val(1) at a low (red) and at a high (blue) volume fraction of TFE. The INLS was extracted from the same datasets as in a). For comparison, the INLS of acetylated proline (30 mg/ml) in D_2O (black, point dashed) and the INLS of ELP90 (20 mg/ml) in D_2O (black, point dashed) is shown.

the ELP1 data sets. The fitting results are summarized in Figure 4.10. We see that the vibrational relaxation rates of the three modes that appear in the model are independent of the solvent composition (Figure 4.10a). Next we consider the exchange dynamics, and interestingly we observe that the two exchange constants show a very different solvent dependence. Apparently the exchange with the Val(1) band (characterized by the exchange constant k_{ba}) is independent of the solvent composition. The other exchange process (i.e. the reshaping of the high-frequency band characterized by the constant k_{cb}), on the other hand, slows down dramatically with increasing TFE concentration.

SPECTRAL DIFFUSION OF THE VAL(1) RESONANCE Finally we again look into the local solvation dynamics of the Val(1) residue. In Figure 4.9b we have plotted the inverse nodal line slope of the Val(1) resonance of ELP1 for the two limiting solvent compositions studied (0% and 60% TFE). As a reference the figure also summarizes the spectral diffusion dynamics of ELP90 (dashed black lined) and AcPro (solid black line). We see that for ELP1 in neat D_2O the spectral diffusion is much slower than was the case for AcPro (whose amide group is fully solvent exposed). Upon increasing the TFE concentration of the solvent these dynamics slow down slightly, and they become very similar to the spectral diffusion dynamics observed in ELP90. We have quantified these observations by fitting a monoexponential to the decay curves, and

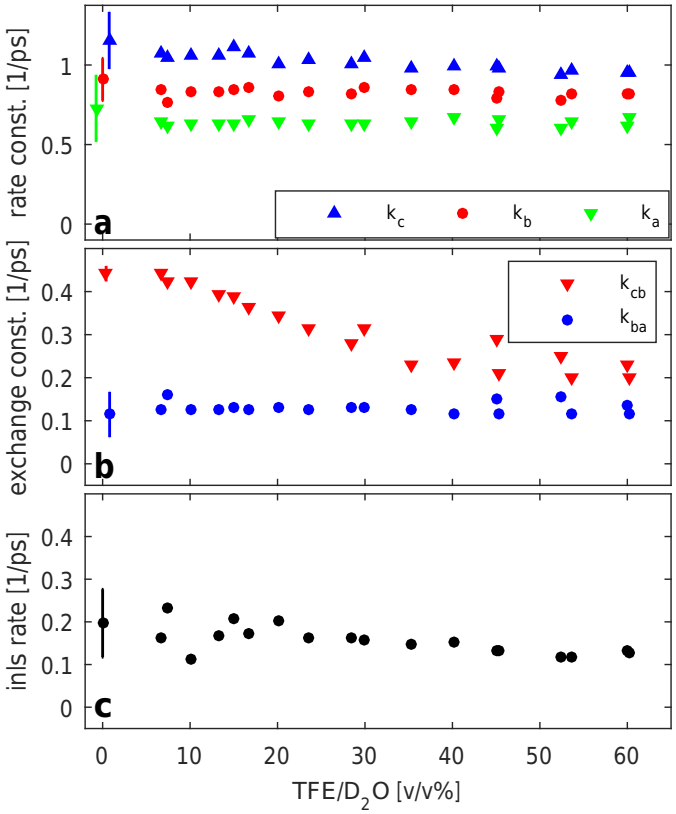

FIGURE 4.10. Fitting results of the relaxation model described in the text to the ELP1 data sets a) Relaxation rates of the three amide I′ modes as a function of the TFE volume fraction. b) Exchange constants k_{cb} and k_{ba} versus TFE volume fractions. c) Decay rate of the spectral diffusion curves of the Val(1) resonance versus TFE volume fraction. The error bars give the standard deviation of the mean of three measurements.

we have plotted the resulting decay constants in Figure 4.10c.

4.4 DISCUSSION

In this work we have performed experiments on two elastin-like peptides. A striking observation is the similar appearance of both the linear and the nonlinear spectra of these two peptides. We have seen that the spectra of ELP1 and ELP90 are accurately described as a superposition of the same three Gaussian bands. As a first point we look into the assignment of these bands. As was already explained, the band at 1615 cm^{-1} is attributed to the Val(1) residue, whose frequency is redshifted due to the adjacent proline residue. The band at 1650 cm^{-1}, on the other hand, is typical of disordered protein structures, so that the question remains what the origin is

Solvent	H-bond type	ELP1 Conformation	
		Extended	Folded
D_2O	peptide-water	12.61 ± 1.77	10.86 ± 1.57
D_2O:TFE	peptide-water	3.88 ± 1.70	3.30 ± 1.52
	peptide-TFE	5.40 ± 2.14	4.31 ± 1.71

TABLE II. Average number of hydrogen bonds per ELP1 molecule in the MD simulations. The errors give the standard deviation.

of the band at 1675 cm^{-1}. A first clue is provided by the fact that for ELP1 the intensity of this band increases upon the replacement of the aqueous solvent for a solvent environment with a lower density of hydrogen bonds (i.e. D_2O:TFE). It is well known that there is a direct correlation between the (local-mode) amide I′ frequency of a residue and the strength of its hydrogen bond.[21,128,129] Therefore a likely explanation for the high-frequency band is that it originates from amino-acid residues which are relatively weakly hydrogen-bonded, either to the solvent or to other amino-acid residues. In order to confirm this interpretation, Ana V. Cunha and Thomas L.C. Jansen performed molecular-dynamics simulations for two ELP1 solutions (in D_2O and in 60% TFE:D_2O), and they measured the number of peptide-solvent hydrogen bonds in these two systems. These simulations were performed for both an extended ELP1 conformation and for a folded ELP1 conformation (i.e. with a hydrogen bond between the two valine residues, see Fig. 4.11). Table II gives the average number of peptide-water and peptide-TFE hydrogen bonds in these simulations. As can be seen the total number of peptide-solvent hydrogen bonds decreases by approximately 30% when the TFE volume fraction is increased from 0 to 60%. This result suggests that the ingrowth of the blue shoulder in the ELP1 spectrum (with increasing TFE volume fraction) can indeed be attributed to a weakening of the average strength of the hydrogen bonds formed by the peptide groups. Another effect that could contribute to the weakening of the *average* hydrogen-bond strength (that is, apart from the presence of a large fraction of broken hydrogen bonds) is the truncation of the water hydrogen-bond network by TFE; this truncation causes the *intact* peptide-water hydrogen bonds to weaken as they are no longer part of an extended network. The spectral similarities between ELP1 and ELP90 strongly suggest that the molecular environment experienced by ELP90 in the coacervate is very similar to environment created by the mixed D_2O:TFE solvent. This means that the spectral changes observed upon the coacervation of ELP90 are very likely attributable to the desolvation of the peptide backbone during the coacervation process. Having assigned the Gaussian bands that appear in our kinetic model, we next consider how to interpret the dynamics observed in the 2DIR spectra. As was described in the previous section there are in essence two delay-dependent processes that can be observed in the 2DIR spectra of ELP1 and ELP90. The first process is the energy exchange between the Val(1) residue and the residues

of the remaining tetrapeptide. The second process is the energy exchange among the residues that form the tetrapeptide. A first point to note is that for ELP90 these two processes occur on the picosecond timescale, both in the solvated and in the aggregated state. The occurrence of picosecond vibrational energy transfer points to a well hydrated structure. The reason is that vibrational energy transfer requires the presence of fluctuations to compensate for the energy mismatch between the modes involved,[69,72,74,130] and these fluctuations are typically provided by the motions of water molecules inside the hydration shell. The fact that energy transfer remains possible in the aggregated state of ELP90 indicates that, despite the desolvation described above, the ELP90 aggregates apparently still contain a relatively large fraction of mobile water molecules. If we examine the rate constants of the exchange processes, we see that for ELP90 the exchange process involving Val(1) does not depend on temperature and the second process slightly slows down with increasing temperature. These observations are mirrored in the ELP1 data where one sees that the Val(1)-exchange is independent of the volume fraction of TFE, while the second process slows down with increasing TFE volume fraction. This slowing down of the energy transfer for ELP1 is likely due to the replacement of light and mobile water molecules in the hydration shell of ELP1 by the heavier and relatively immobile TFE molecules. An additional effect that plays a role here is the fact that TFE molecules are known to preferentially aggregate around peptides,[119,131] so that TFE is very effective at displacing water molecules. Another interesting observation is the fact that for both ELP90 and ELP1 $k_{cb} > k_{ba}$. That is, energy transfer proceeds more slowly whenever the Val(1) residue is involved. A likely explanation could be that for this exchange process the frequency mismatch is relatively large, i.e. larger than the typical magnitude of the frequency fluctuations.

Given that for ELP1 the exchange constant k_{cb} is sensitive to the degree of hydration, it would be interesting to use the ELP1 data as a reference and to estimate the degree of desolvation that occurs during the aggregation of ELP90. This can be done as follows. For ELP90 the rate constant k_{cb} decreases by about 20% upon aggregation of the peptide (Table I). In order to achieve a similar decrease for ELP1 the volume fraction of TFE needs to be ~25% (Figure 4.10). Because of the preferential aggregation of TFE, mentioned above, this actually corresponds to an even higher TFE concentration inside the solvation shell of ELP1. The MD simulations were used to calculate the preferential aggregation of TFE around the folded ELP1 peptide assuming a solvation shell of 0.6 nm, identically to ref.[119] The first solvation shell concentration of TFE was found to be 3.0 times higher than the bulk concentration, which is similar to previous findings for other proteins.[119] Using this result we find that for an ELP1 solution in 25% D_2O:TFE the TFE volume fraction inside the solvation shell is as large as 75%, which means that the concentration of water molecules is only 25% of the bulk value. From this we conclude that during the aggregation of ELP90 roughly 3 out of 4 water molecules are displaced from its solvation shell.

We end the discussion of our results by turning to the spectral diffusion dynamics of the Val(1) residue, which are displayed in Figures 4.4 and 4.9. The decay of the inverse nodal line slopes shown in these figures directly reflects the degree of solvent exposure of the Val(1) residue. As can be seen from the black curve in Figure 4.4b a

fully solvent exposed residue, such as the amide group of AcPro, exhibits a complete decay of the nodal line slope on a ∼2 ps timescale. In contrast, for ELP90 we observe a much slower decay of the nodal line slope, which indicates that in this peptide the Val(1) residue is shielded from the solvent. A likely explanation for this strong shielding from the solvent is that the C=O group of the Val(1) residue may form an intrapeptide hydrogen bond with the NH group of the Val(4) residue. The presence of such a hydrogen bond is in line with the notion that the Pro-Gly sequence is often located inside a β-turn.[132,133] The molecular dynamics simulations were used to further investigate this interpretation of our experimental results. For both simulated conformations the frequency-frequency correlation function (FFCF) of the Val(1) residue was computed. It turns out that on the timescale of the simulations (10 ns) these two conformers do not interconvert, i.e. the peptide maintains the conformation chosen at the start of the simulation. Figure 4.11 displays the FFCF for these two simulations. If we compare the simulation of the folded and extended structures (in water), we see that indeed the presence of the β—turn causes a slowing down of the decay of the FFCF, which corroborates our interpretation. We further note that for the folded structure the replacement of the aqueous solvent by a TFE:water mixture leads to an upward shift of the simulated FFCF, and this observation is again in line with our experimental observation (Fig. 4.9). Interestingly, our experiments show that the spectral diffusion dynamics and thereby the degree of solvent shielding are identical in the dissolved and aggregated state of ELP90 and show very little change in ELP1 as a function of TFE concentration. This implies that the β-turn is present in both states of the peptide, and therefore we conclude that contrary to suggestions found in the literature[134–137] the coacervation transition of elastin-like peptides may not be driven by the formation of a β-turn. Instead we speculate that the role of the β-turn may be more indirect: that is to say, the β-turn may stabilize a conformation in which a large number of hydrophobic sidechains are exposed, so that hydrophobic association can occur once the driving force (and therefore the temperature) is high enough.

4.5 CONCLUSION

We used linear infrared spectroscopy, 2DIR spectroscopy and MD simulations to study the structural dynamics of elastin-like peptides (ELP). To gain insight into the coacervation transition displayed by this class of peptides we performed experiments on two different ELPs. We studied a 90-repeat ELP (450 residues), for which coacervation can be induced by increasing the temperature above the transition point. We also performed reference measurements on a single-repeat ELP (5 residues). This ELP was too short to show a coacervation transition, and therefore in this case experiments were performed as a function of the solvent composition (i.e. different volume fractions of TFE in water).

Our results show that for both peptides the amide I′ spectrum can be well described as a superposition of three Gaussian bands located at 1615 cm^{-1}, 1645 cm^{-1} and 1675 cm^{-1}. We assign the 1615 cm^{-1} band to the localized amide I′ resonance of the Val(1) residue. The 1645 cm^{-1} and the 1675 cm^{-1} bands are associated with

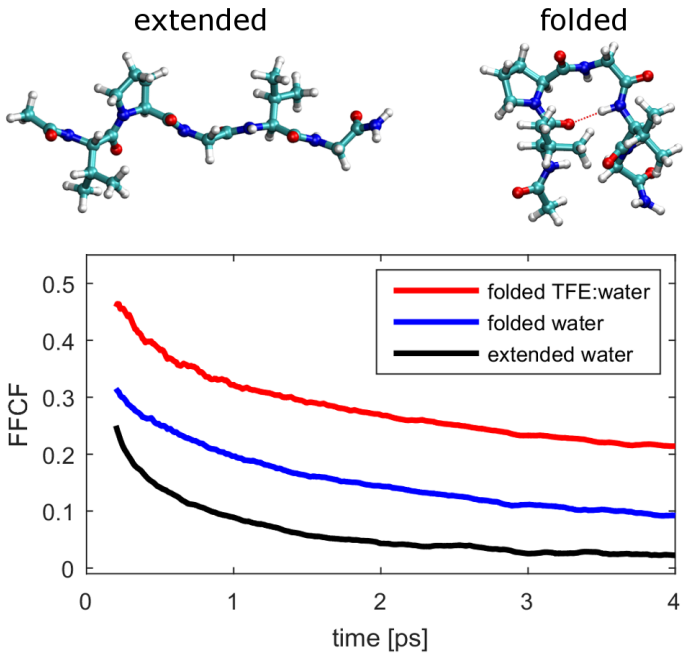

FIGURE 4.11. Frequency-frequency correlation function (FFCF) of the amide I′ vibration of Val(1) in ELP1 extracted from MD simulations. The simulations were performed for an extended and hydrogen bonded confirmation (see top) in two different solvents (water and TFE:water).

residues 2 to 5 in the pentapeptide repeat and probably have a more delocalized character. We attribute the 1645 cm^{-1} band to well-hydrated residues and the 1675 cm^{-1} band to more weakly hydrated residues. In the 2DIR experiments we have identified two vibrational energy transfer processes that take place between the three bands. One of these transfer processes is independent of the solvent environment of the peptides while the second process slows down when water molecules in the solvent are replaced by TFE for ELP1 or when the temperature is raised above the coacervation temperature for ELP90. We use the solvent-dependent process to estimate the degree of desolvation that takes place upon coacervation of 90-repeat ELP, and we find that this desolvation corresponds to a loss of roughly three out four water molecules in the hydration shell.

Finally we studied the spectral-diffusion dynamics of the Val(1) residue. We find that these dynamics are very slow and indicative of an amide group that is shielded from the solvent. Surprisingly, for the 90-repeat ELP these dynamics do not change with the aggregation state of the peptide. We conclude that the slow dynamics are likely due to the fact that the Val(1) residue forms an intrapeptide hydrogen bond with the Val(4) residue (β-turn), already below the coacervation transition.